Engineering Tripos Part IB, Paper 2P3 – Materials, 2024: Solutions

H.R. Shercliff / A.E. Markaki / M. Seita

Q1 (a) (i) The solid and liquid phases have distinct free energy curves that intersect, defining the equilibrium temperature, T_m (the solid and liquid phases are in equilibrium). The stability domains of the liquid and solid phases are shown in the schematic below. For temperatures below T_m, the solid phase has the lowest free energy and is therefore the stable equilibrium phases. Conversely, at temperatures above T_m, the liquid phase is stable.

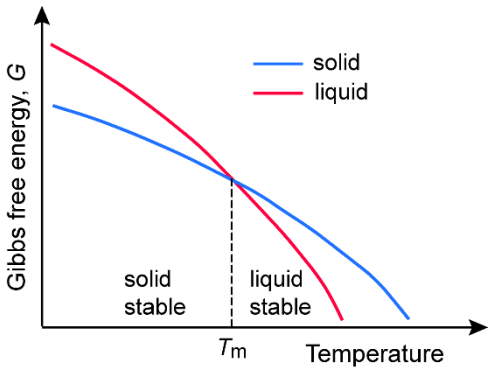

(ii) The Gibbs free energy ΔG is given by $\Delta G = \Delta H - T\Delta S$, where ΔH and ΔS are the change in enthalpy and entropy respectively.
At T_m (and for a fixed pressure), ΔG must be zero. Assuming that ΔH and ΔS do not vary significantly with temperature (this is a reasonable assumption: although the absolute values of enthalpy and entropy are dependent upon temperature, the *differences* between the 2 phases will be weak functions of temperature):

$\Delta G(T_m) = \Delta H - T_m \Delta S = 0 \Longrightarrow \Delta S = \Delta H/T_m$
$\Delta G(T) = \Delta H - T\Delta S = \Delta H - T\Delta H/T_m$
$\therefore \Delta G(T) = \Delta H \left(\frac{T_m - T}{T_m}\right)$
$\Delta G(T)$ varies to the first order with $T - T_m$ (undercooling / supercooling).

Alternatively you could also use the following:
At T_m, $\Delta G = \Delta H - T_m \Delta S = 0$, hence $\Delta H = T_m \Delta S$
$\Delta G(T) = T_m \Delta S - T\Delta S = \Delta S \left(T_m - T\right)$

(b) Interstitial solid solutions have smaller atoms that fit into the 'holes' between larger atoms (e.g. C in Fe), while substitutional solid solutions have similar-sized atoms that replace each other in the crystal lattice (Zn in Cu).

Interstitial solutes diffuse by motion of the *small* solute atom from one interstitial site to the next. *i.e.* the solute atoms move via the gaps between the solvent atoms.

Substitutional solutes diffuse via motion of the solute atom from a substitutional site to an adjacent vacant site. Relevant to atoms of *similar atomic size*. Atomic motion only occurs if a vacancy is available.

Both interstitial and substitutional diffusion can be thought of as requiring the diffusing atom to squeeze through a small gap. It requires the solute atom to move from one (low energy) lattice site to the next, via a position in which its energy is higher. Hence, to diffuse, the atom must overcome an energy barrier, equal to the increase in energy from the low to the high energy site. This energy barrier q is the activation energy for diffusion, $Q = q\, N_A$ (J/mol, N_A is the Avogadro's number), as sketched above.

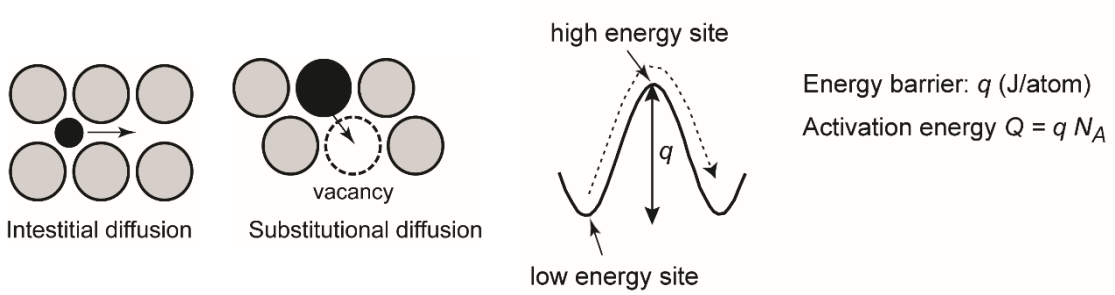

Since interstitial atoms almost always have an adjacent empty interstitial site to move into, interstitial diffusion is faster than substitutional diffusion, which requires a vacancy to be available.

(c) $D = D_0 \exp(-Q/RT)$ $T_1 = 330+273 = 603$ K $T_2 = 730+273 = 1003$ K

$$D(T_1) = 8.2 \times 10^{-22} = D_0 \exp(-Q/RT_1)$$

$$D(T_2) = 3.6 \times 10^{-15} = D_0 \exp(-Q/RT_2)$$

If you divide the two equations and take natural logs, the resulting equation is

$$\ln\left(\frac{D(T_1)}{D(T_2)}\right) = \left(-\frac{Q}{R}\right)\left(\frac{1}{T_1} - \frac{1}{T_2}\right)$$

Solving for Q

$$Q = -R \ln\left(\frac{D(T_1)}{D(T_2)}\right)\left(\frac{1}{\left(\frac{1}{T_1} - \frac{1}{T_2}\right)}\right) = -8.314 \ln\left(\frac{8.2 \times 10^{-22}}{3.6 \times 10^{-15}}\right)\left(\frac{1}{\left(\frac{1}{603} - \frac{1}{1003}\right)}\right)$$

$$\therefore Q = 192271 \text{ J mol}^{-1} \approx 192 \text{ kJ mol}^{-1}$$

(d) In a single crystal sample diffusion would be expected to occur principally through the bulk substitutional diffusion mechanism described above. In a polycrystalline sample, a higher diffusion rate would be expected because the grain boundaries provide faster diffusion paths. In the single crystal there may be dislocations, which would also give short circuit diffusion paths, but this is also true for the polycrystalline sample.
Table 1 shows that the diffusion coefficient is significantly higher in the polycrystalline sample at the lower temperature (330 °C) but at the higher temperature (730 °C) they are very similar. This suggests that grain boundary diffusion dominates at the lower temperature and, at the higher temperature, the same bulk diffusion mechanisms are dominant in both samples. It is possible that there may be significant grain growth at higher temperatures, leading to a reduction in grain boundary area and hence similar D values to the single crystal sample.

Q2 (a) Oxidation occurs when the Gibbs free energy of reaction ΔG^0 , the free energy difference between the oxide (product) and metal and oxygen (reactants) at a particular temperature and pressure, is less than zero ($\Delta G^0 < 0$). (If $\Delta G^0 > 0$, the metal surface is stable (no oxidation)).

At short time-scales, the oxide layer is very thin. The rate limiting step in the formation of an oxide layer is dependent on the diffusion of reactants (oxygen ions, metal ions) through the oxide thickness, and their relative diffusivities. This leads to a constant growth rate. At long time scales, oxides often follow a parabolic growth rate because the rate limiting process becomes the diffusion across the oxide layer when this layer is thick enough.

Linear kinetics occur when the oxide evaporates (linear loss) or cracks, peels off (linear gain) allowing oxygen to reach freely the metallic surface for further oxidation.

(b) (i) Under the curve there are approximately 85 squares, with height of 0.2 microns and width of 5 mm. Hence the oxide volume will be:

$2\pi r \times (85 \times 5 \times 10^{-3} \times 0.2 \times 10^{-6}) \approx 2.67 \times 10^{-9}$ m^3

where r is the tube radius (5×10^{-3} m)

From Figure 1, at 400 °C, volume at this end of the bar will be

$\approx \pi r^2 \times 0.2 \times 10^{-6}$ m $= 1.57 \times 10^{-11}$ m^3

At 500 °C, volume at the other end of the bar $\approx \pi r^2 \times 1.9 \times 10^{-6}$ m $= 1.50 \times 10^{-10}$ m^3

Hence oxide mass $\approx 6 \times 10^6$ g/m^3 $\times$ (2.67+ 0.0157 + 0.150) $\times$ 10^{-9} m^3 $\approx$ 17 mg

(ii) A total oxide mass of 85 mg is 5× the mass of oxide found in part (b) for a period of 1 hour. Assuming the oxide follows a parabolic rate equation and that the rate of oxidation doesn't change with time, then it would take 25× longer time compared to part (b), hence 25 hours.

(iii) If the oxide thickness follows a parabolic law, then: $y\,(t)^2 = C_1\, t + C_2$. At time $t = 0$, $y = 0$, hence $C_2 = 0$.

Arrhenius law states that rate of process $\propto$ – exp (Q/R), where Q is the activation energy and R is the universal gas constant (8.314 J mol^{-1} K^{-1}).

We have a linear temperature profile along the bar, so from Figure 1 we know the oxide thickness as a function of temperature.

Temperature T (°C)	T (K)	y (μm /1 hr)	Rate: $y^2/3600$ (m^2 s^{-1})
400	673	0.2	$(0.2\times10^{-6})^2/3600$
420	693	0.4	$(0.4\times10^{-6})^2/3600$
440	713	0.6	$(0.6\times10^{-6})^2/3600$
460	733	0.9	$(0.9\times10^{-6})^2/3600$
480	753	1.3	$(1.3\times10^{-6})^2/3600$
500	773	1.9	$(1.9\times10^{-6})^2/3600$

To find the activation energy Q, the data should be plotted as ln (rate) vs $1/T$ (T in Kelvin).

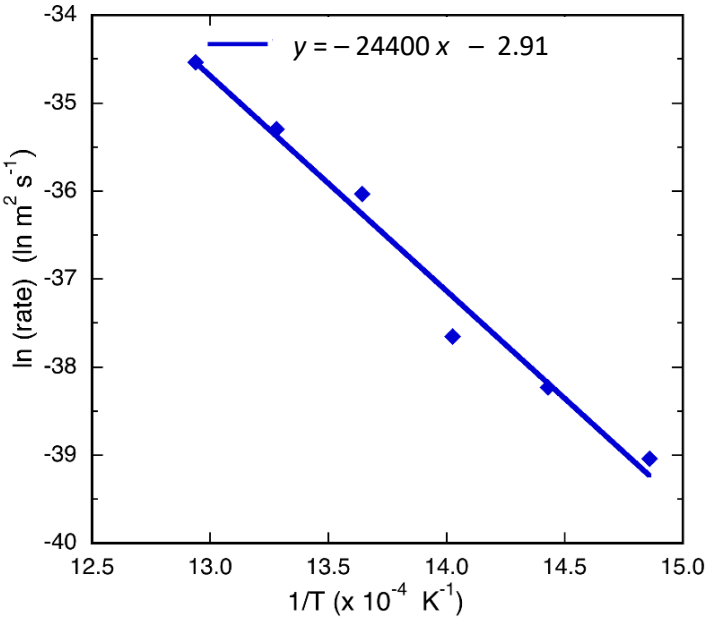

The slope is $Q/R \approx 24400$ J mol^{-1} hence $Q \approx 203$ kJ mol^{-1}.

Q3

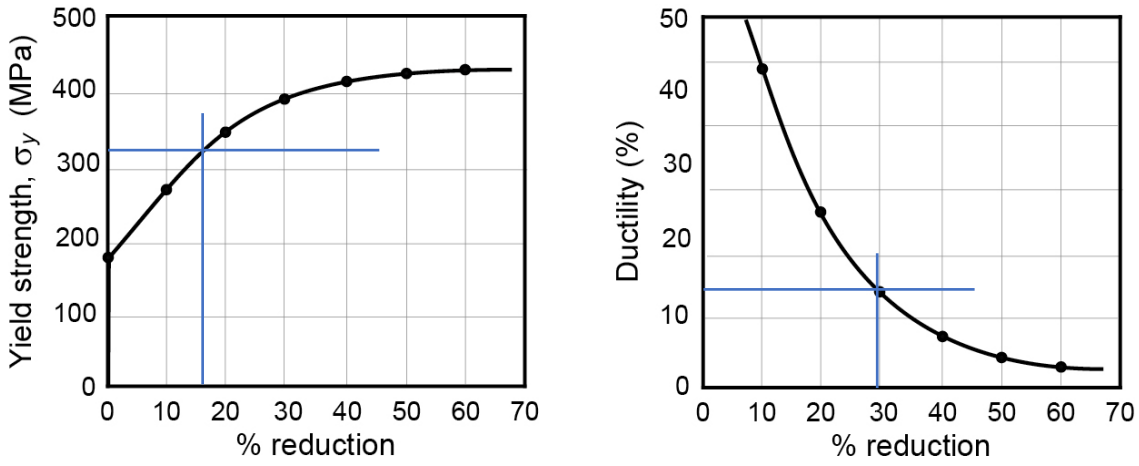

(a) (i) A thickness reduction to 0.8 mm would result into a nominal plastic strain of:

$\varepsilon_n = \frac{t_f}{t_0} - 1 = \frac{0.8}{1.34} - 1 = -0.40$, a reduction of 40%.

From Fig. 2, the ductility of brass after 40% reduction is ~8%, which does not satisfy the property specification.

(ii) From Fig. 2 above, the possible range of plastic strain which can be applied to the annealed alloy in the second pass, in order to satisfy the requirements on yield strength and ductility are:

Minimum strain to meet strength target (ductility fine): ~17%

Maximum strain to meet ductility target (strength fine): ~30%.

The corresponding intermediate sheet thicknesses between the two passes will be:

For a 2nd pass reduction of 17%: $\varepsilon_n = -0.17 = \frac{0.8}{t_{int}} - 1$, hence $t_{int} = 0.96$ mm

Hence magnitude of first pass reduction: $\varepsilon_n = \frac{0.96}{1.34} - 1 = -0.28$, or 28% reduction

For a 2nd pass strain of magnitude 30%: $\varepsilon_n = -0.30 = \frac{0.8}{t_{int}} - 1$, hence $t_{int} = 1.14$ mm

Hence magnitude of first pass reduction: $\varepsilon_n = \frac{1.14}{1.34} - 1 = -0.15$, or 15% reduction

(iii) For equal magnitudes of % reduction in each pass, the intermediate sheet thickness must satisfy:

$\varepsilon_n = \frac{t_{int}}{1.34} - 1 = \frac{0.8}{t_{int}} - 1$, i.e. ${t_{int}}^2 = 1.34 \times 0.8$

Hence the intermediate thickness $t_{int} = 1.04$ mm

The % reduction in each pass is then $\varepsilon_n = \frac{1.04}{1.34} - 1 \approx -0.22$, or 22% reduction

The yield strength and ductility of the sheet after the second pass to this % reduction are ~360MPa and ~20%, respectively.

(b) (i) For a nominal strain of –22%, the true strain is: $\varepsilon_t = \ln(1 - 0.22) = -0.25$
The true stress-strain response is the same in tension or compression, hence the flow stress at this magnitude of true strain is: $\sigma_t = 180 + 380\ (0.25)^{0.3} = 431$ MPa.

(ii) Work done during the first rolling process:

$$W = \int_0^{0.25} 180 + 380 \cdot \varepsilon^{0.3}\, d\varepsilon = 180 \cdot 0.25 + \frac{380}{(0.3+1)} \cdot 0.25^{(0.3+1)} = 45.7 \text{ MJ/m}^3$$

(iii) 5% of the plastic work done is: $0.05 \times 44.7 = 2.25$ MJ/m^3

The remaining 95% is dissipated through heat.

The energy stored per unit length of dislocation is: $E_\perp = Gb^2/2$

i.e. $E_\perp = (33 \times 10^9) \times (0.275 \times 10^{-9})^2/2 = 1.25 \times 10^{-9}$ J/m

Hence the estimated dislocation density ρ_d in the material after applying $\varepsilon_t = 25\%$ is:

$$\rho_d = \frac{2.25 \times 10^6}{1.25 \times 10^{-9}} = 1.8 \times 10^{15} \text{ m/m}^3$$

Q4 (a) Hardenability is defined as the ability of a steel to form martensite on quenching from the austenite field, as a pre-requisite for tempering. In practical terms, it limits the size of component that can form 100% martensite right through the thickness, to the point of slowest cooling. It may be quantified for a given steel by the diameter of solid cylinder that reaches a minimum fraction of martensite at its centre (or by the Jominy end-quench – see below).

(b) (i) The characteristic heat flow distance in a time t is given by $\sqrt{at}$ where a is the thermal diffusivity. For a distance $x = \sqrt{at}$, erf(X) = erf(½) ≈ ½, i.e. when the temperature has dropped by about half of the cooling interval. From the shape of the error function, the length L of the bar needs to be many multiples of $\sqrt{at}$ for the bar to be treated as semi-infinite.

(Figure not expected: $\sqrt{at} \ll L$ is an acceptable answer, but from the figure a factor of 4-5× is sufficient).

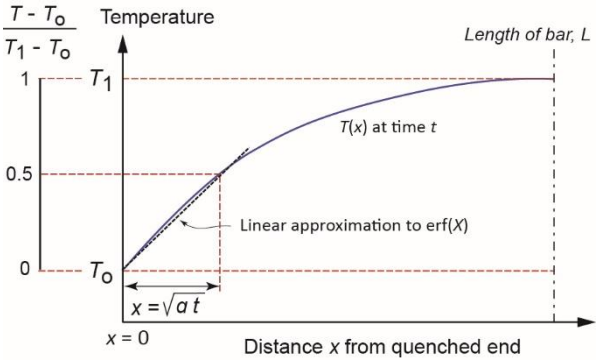

(ii) For $X < 0.7$, erf(X) ≈ X, so $\frac{T(x,t) - T_0}{T_1 - T_0} \approx \frac{x}{2\sqrt{at}}$

For a reference temperature T_r, the time taken to reach it is: $t_r = \frac{x^2}{4a}\left(\frac{T_1 - T_0}{T_r - T_0}\right)^2$

(iii) $\Delta T = (T_{r1} - T_{r2})$

$$\Delta t = \frac{x^2}{4a}\left[\left(\frac{T_1 - T_0}{T_{r2} - T_0}\right)^2 - \left(\frac{T_1 - T_0}{T_{r1} - T_0}\right)^2\right]$$

Average cooling rate between T_{r1} and T_{r2} is $\Delta T/\Delta t$:

$$\frac{\Delta T}{\Delta t} = \frac{4a\,(T_{r1} - T_{r2})}{x^2}\left[\left(\frac{T_1 - T_0}{T_{r2} - T_0}\right)^2 - \left(\frac{T_1 - T_0}{T_{r1} - T_0}\right)^2\right]^{-1}$$

All the temperatures, and the thermal diffusivity a are constants, so $\frac{\Delta T}{\Delta t} = \frac{C}{x^2}$: see figure.

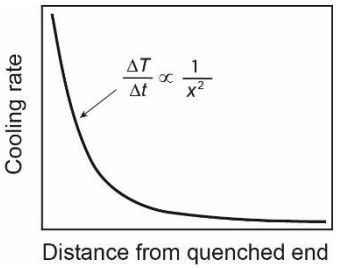

(iv) The temperature interval 700 to 500 °C spans the 'nose' of the TTT diagram, where the transformation to ferrite and pearlite is fastest – hence this is the critical part of the cooling history when the goal is to *avoid* these transformations to form martensite.

$T_1 - T_0 = 1000 - 20 = 980$°C

$T_{r1} - T_{r2} = 700 - 500 = 200$°C

$(T_1 - T_0) / (T_{r2} - T_0) = 980/(500 - 20) = 2.042$

$(T_1 - T_0) / (T_{r1} - T_0) = 980/(700 - 20) = 1.441$

$a = 10^{-5}$ m^2/s

Substituting into the cooling rate equation:

$$\frac{\Delta T}{\Delta t} = \left(\frac{1}{x^2}\right) 4 \times 10^{-5} \times 200 \times [2.042^2 - 1.442^2]^{-1} = \frac{0.003825}{x^2}$$

For a = 1mm = 10^{-3} m, cooling rate = 3830 °C/s

For a = 30mm = 3×10^{-2} m, cooling rate = 4.25 °C/s

(v) In Figure 7.2 in the Materials Databook (plain C steel), the hardness is very high near the quenched end, indicating martensite, but falls rapidly to a much lower value by 30mm – at the lower cooling rate, ferrite and pearlite are formed. In Figure 7.4 (low alloy steel), the high hardness is maintained right along the bar: martensite is formed throughout, at much lower cooling rates. The low alloy steel has the higher hardenability.

(c) For some distance from the quenched end, the cooling rate is fast enough to miss the C-curves for precipitation of coarse, equilibrium phases. The result is a supersaturated solid solution, with a moderate hardness. Far from the end, the cooling rate is low and equilibrium phases form, giving negligible precipitation hardening and using up all of the solute – the hardness is low (effectively the same as the overaged state). There is a smooth transition between the two with increasing distance (falling cooling rate) as some coarse precipitation occurs, and the supersaturation falls below 100%.

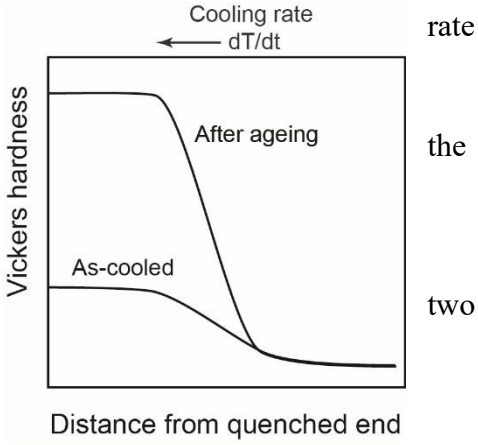

After ageing, the supersaturated region fully age hardens to the peak hardness. Far from the end there is no change – it is already overaged. In the transition zone, the available supersaturated solute leads to age hardening, but progressively falling in hardness due to the depleted supply of solute after the original cooling.

Q5 (a) Medium C steels are Fe with around 0.3 – 0.5 wt% C – the phase diagram shows the cooling path for 0.3 wt% C.

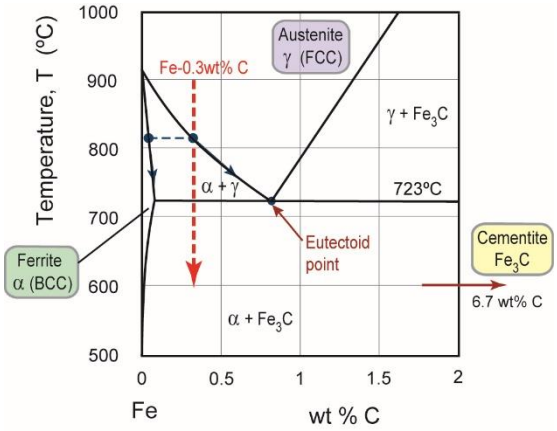

(i) Normalisation:

Starting with 100% FCC austenite at 900°C, at 780 – 810 °C (depending on the C content), BCC ferrite nucleates on the austenite grain boundaries, rejecting C into the remaining austenite (as BCC dissolves a low amount of C).

If equilibrium is followed, the proportions of ferrite: austenite reach about 50:50 when the temperature reaches the eutectoid temperature, 723 °C. The remaining austenite, containing 0.8 wt% C, transforms to the phases ferrite and iron carbide, in a plate-like microstructure in grains of pearlite (nucleating and growing from existing grain boundaries).

Key mechanisms:

From 800 to 723°C: ferrite nucleating from austenite grain boundaries; growth of ferrite by atomic transfer across the FCC-BCC boundary.

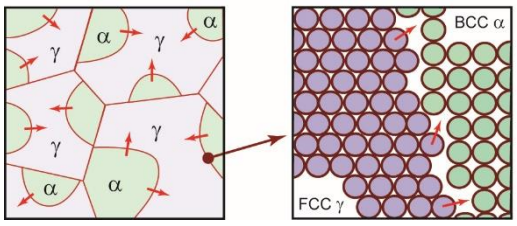

Eutectoid transformation (across 723°C):

Pearlite nucleation and growth require FCC austenite (0.8 wt% C) to simultaneously transform into (low C) BCC ferrite and iron carbide (Fe_3C). The new phases grow in parallel plates to minimise the diffusion distance of C at the austenite–pearlite interface.

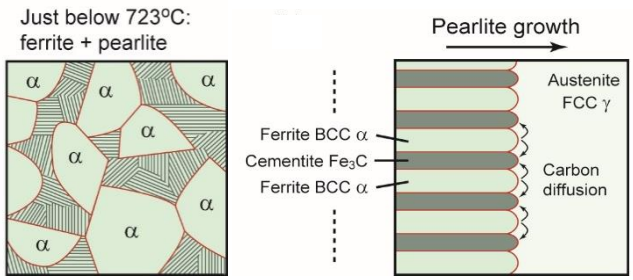

(ii) Quenching:

Starting with 100% FCC austenite at 900°C, martensite forms over a temperature interval well below the eutectoid temperature (around 300 °C). No diffusion is involved – needle-like grains of martensite nucleate on the austenite grain boundaries, and cross the grains at very high speed by a displacive transformation that changes FCC iron to BCC by imposing a shear strain. Needles progressively form in large numbers until the austenite grains have been consumed. The carbon remains in supersaturated solution in the BCC lattice.

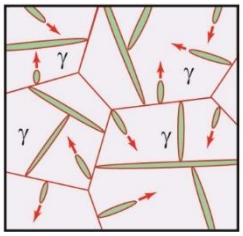

(b) The chart shows likely positions of 0.4 wt% C after the 3 heat treatments, with the values explained as follows:

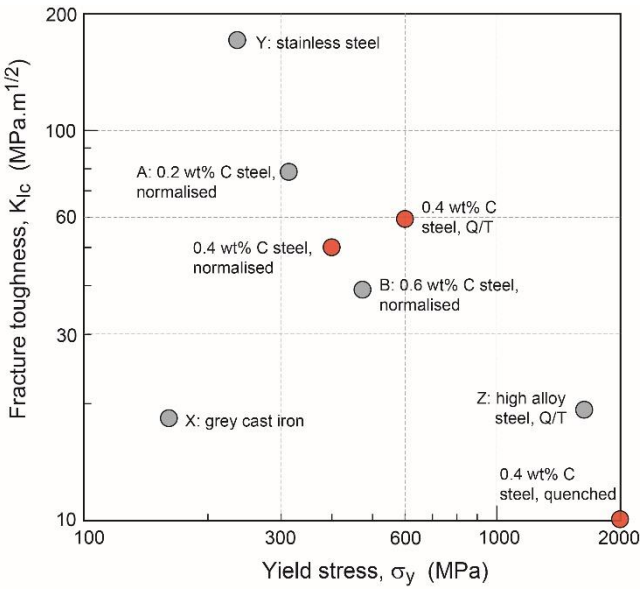

(i) Normalised: the microstructure consists of grains of ferrite and pearlite, with almost all the carbon in the iron carbide within the pearlite. So going from to 0.6 wt% C, the proportion of iron carbide and this pearlite increases in proportion. Iron carbide is the hard phase, the yield stress lies between A and B. Similarly, the pearlite plates offer the easiest route for crack propagation, while ferrite is most resistant – so the fracture toughness will also lie between A and B.

0.2

so

(ii) After quenching, 100% martensite is formed. The toughness is near zero; the yield stress is high compared to ferrite and pearlite, by a factor of 4-5.

(iii) After quenching and tempering, iron carbide precipitates and the martensite lattice relaxes to equilibrium ferrite. The precipitates are fine scale, and all the grains have the same microstructure. The yield stress is higher than in the normalised condition (typically by 50%), and the avoidance of plates of iron carbide (as in pearlite) also enhances the fracture toughness.

(c) X is grey cast iron: the microstructure is coarser than a normalised steel, with carbon forming graphite flakes. This limits the fracture toughness, while the yield stress is low due to the coarse scale of the second phases (iron carbide and graphite).
Applications: drain covers, disk brakes, ornamental railings.
Design requirements: low cost, complex 3D shapes.

Y is stainless steel: the microstructure is (usually) austenitic (FCC), hardened by high solid solution levels and work hardening, not precipitation hardening – this gives an average yield stress, but very high fracture toughness.
Applications: chemical/cryogenic pipework/pressure vessels, cutlery.
Design requirements: corrosion resistance.

Z is quenched/tempered high alloy steel: medium to high C, with high additions of alloying elements (Mo, V, W). Alloying gives high hardenability (enabling air cooling to minimise thermal stresses during quenching), high solid solution strength, and the formation of fine-scale tempered microstructure, with alloy carbides giving high precipitation hardening. Hence yield stress if very high (including at temperature), while uniform fine-scale microstructure gives moderate fracture toughness.
Applications: cutting tools
Design requirements: quite complex shapes with sharp cutting edges.

Q6

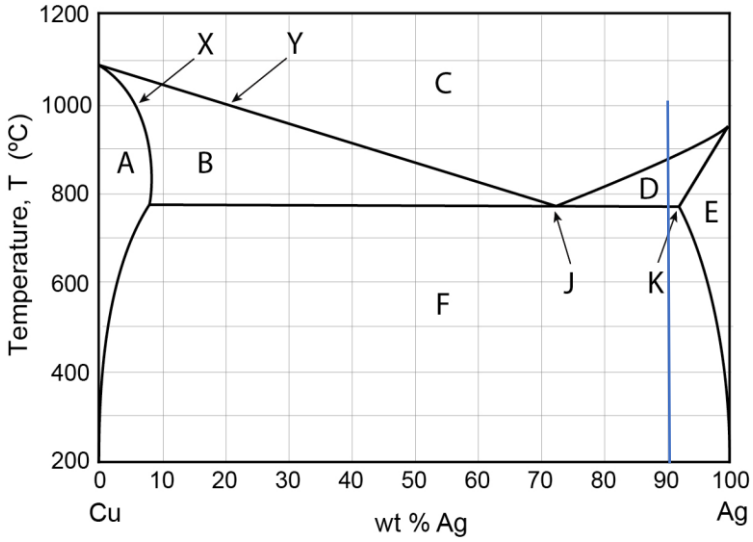

(a) (i)

A. Cu-rich single solid phase (α)
B. 2-phase field (α and Liquid)
C. Single Liquid phase
D. 2-phase field (β and Liquid)
E. Ag-rich single solid phase (β)
F. 2-phase solid field (α and β)

(ii) X: Solidus line, indicating the higher boundary of the solid phase field (α), below which the alloy has completely solidified.

Y: Liquidus line, indicating the lower boundary of the liquid phase field, below which the solid phase nucleates.

Segregation refers to the rejection of solute from the growing solid phase into the liquid because of solute partitioning: the solid that forms from a given composition of liquid is purer than the liquid. In equilibrium solidification, the composition of the solid and the liquid both increase as the temperature falls in the liquid + solid field. In reality, however, this is often not the case because of slow diffusion of solute back into the solid, so a gradient of concentration is built up from centre to the outside of the grains. The highest concentration of solute is found at the grain boundaries.

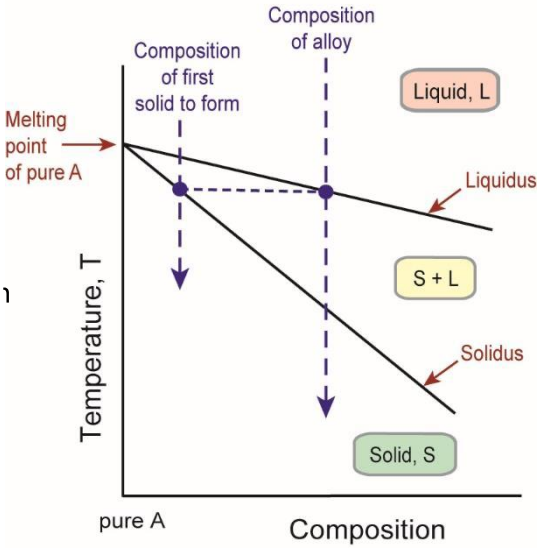

(b) (i) As the melt cools down below ~880°C, the first solid β-phase nucleates in the liquid. Initially, the nuclei are purer compared to the nominal alloy composition, but they incorporate more Cu as the temperature decreases (and as they grow). At a temperature of ~780°C, just above the eutectic temperature, only a small fraction of liquid remains in the microstructure (~10 wt%). Just below the eutectic temperature, this liquid transforms into the eutectic microstructure α + β, with a characteristic needle-like/lamellar structure. On further cooling, the α and β components within the eutectic microstructure become purer and the phase fractions adjust. Precipitation of Cu-rich α may take place within the β grains, which are increasingly supersaturated in Cu as the temperature falls (this depends on the ease with which nuclei of α can form).

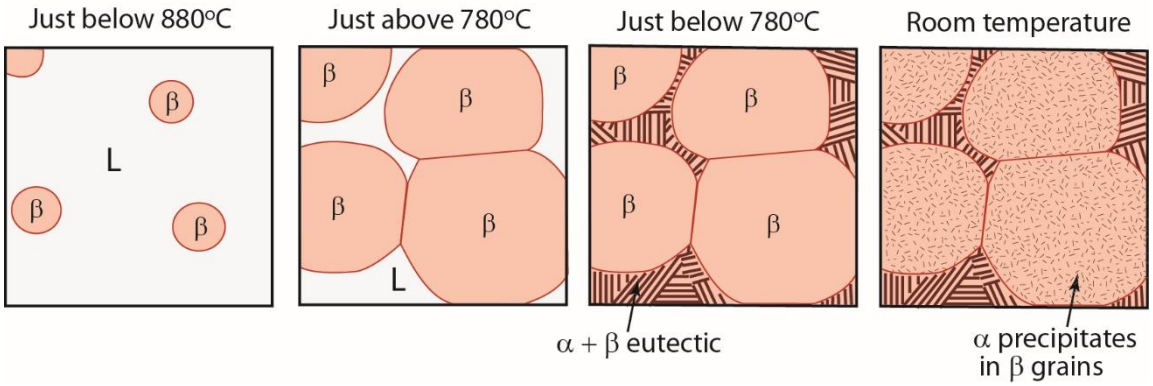

(ii) No significant differences except from some coarsening of the α precipitates in the β grains. This is because the microstructure is already at equilibrium. But coarsening precipitates would potentially lead to a drop in yield stress.

(c) (i) J indicates the eutectic composition for this Cu-Ag alloy. At this composition, the alloy solidifies completely as its temperature decreases below the (eutectic) temperature of 779°C. Since there is no freezing range, this composition is ideal for casting because the melt has low viscosity. It is also the lowest temperature at which 100% liquid can be formed – energy-efficient reducing costs, and increasing productivity.

(ii) The alloy composition corresponding to point K indicates the maximum solubility limit of β. If an alloy with this composition is cooled rapidly and then aged at a temperature below the solvus line, it may form a high density of Cu-rich precipitates which will strengthen the alloy.